

AD-A249 380



REPORT DOCUMENTATION PAGE

Form Approved
OMB No. 0704-0188

(2)

Information is estimated to average 1 hour per response, including the time for reviewing instructions, searching existing data sources, completing and reviewing the collection of information. Send comments regarding this burden estimate or any other aspect of this form for reducing this burden, to Washington Headquarters Services, Directorate for Information Operations and Reports, 1215 Jefferson Avenue, Washington, DC 20503, and to the Office of Management and Budget, Paperwork Reduction Project (0704-0188), Washington, DC 20503.

1. REPORT DATE 03-15-92		3. REPORT TYPE AND DATES COVERED Final 07-01-91 to 3-15-92	
4. TITLE AND SUBTITLE A Microprism Array for Large-Scale, Wide-Band Interconnection of Optoelectronic Systems		5. FUNDING NUMBERS DAAL03-91-C-0030	
6. AUTHOR(S) Ray Chen, Ph.D			
7. PERFORMING ORGANIZATION NAME(S) AND ADDRESS(ES) Physical Optics Corporation 20600 Gramercy Place, Suite 103 Torrance, CA 90501		8. PERFORMING ORGANIZATION REPORT NUMBER Final 3128	
9. SPONSORING/MONITORING AGENCY NAME(S) AND ADDRESS(ES) U.S. Army Research Office P.O. Box 12211 Research Triangle Park, NC 27709-2211		10. SPONSORING/MONITORING AGENCY REPORT NUMBER ARO 290051-EGS01	
11. SUPPLEMENTARY NOTES The view, opinions and/or findings contained in this report are those of the author(s) and should not be construed as an official Department of the Army position, policy, or decision, unless so designated by other documentation.			
12a. DISTRIBUTION/AVAILABILITY STATEMENT Approved for public release; distribution unlimited.		12b. DISTRIBUTION CODE	
13. ABSTRACT (Maximum 200 words) <div style="display: flex; justify-content: space-between;"><div style="width: 30%; text-align: center;">DTIC ELECTE S D APR 30 1992</div><div style="width: 65%;"><p>Technical Abstract (Limit your abstract to 200 words with no classified or proprietary information data)</p><p>In contrast to any existing means of interconnection for a large-scale, high-speed optoelectronic system, Physical Optics Corporation (POC) proposes fabricating and using a microprism (~100 µm in size) array (MPA) as a wide-band coupler for two-dimensional and three-dimensional system integration. The flexibility of MPA's angles allows implementation of the MPA to any point to point interconnects. Realizing that the major bottle neck of hologram-based interconnection is the intrinsic <u>limitation of coupling bandwidth</u> (~10 µm), we demonstrated a microprism coupler (MPA) with larger than 200 µm bandwidth from free space to optical data bus (ODB). For example, LED-based transmission from a single-mode guide to a multi-mode fiber can be solved only by using the MPA. Unlike the conventional prism which has a dimension of ~mm to ~cm, the MPA has miniscule dimensions. An MPA with ~100 µm in size was demonstrated. The proposed MPA is immune from electromagnetic interference (EMI). Furthermore, the cost of the microprism is less than \$1 a piece in mass production, significantly less than holograms.</p><p>In Phase I, fabrication of the MPA will be upgraded followed by a demonstration of large-scale board-to-board MAP-based 3-D interconnection.</p></div></div>			
14. SUBJECT TERMS Microprism, Optical interconnect wide band coupler		15. NUMBER OF PAGES 30	
		16. PRICE CODE	
17. SECURITY CLASSIFICATION OF REPORT UNCLASSIFIED	18. SECURITY CLASSIFICATION OF THIS PAGE UNCLASSIFIED	19. SECURITY CLASSIFICATION OF ABSTRACT UNCLASSIFIED	20. LIMITATION OF ABSTRACT UL

DISCLAIMER NOTICE



THIS DOCUMENT IS BEST QUALITY AVAILABLE. THE COPY FURNISHED TO DTIC CONTAINED A SIGNIFICANT NUMBER OF COLOR PAGES WHICH DO NOT REPRODUCE LEGIBLY ON BLACK AND WHITE MICROFICHE.

Approved for Public Release
Distribution Unlimited

A MICROPRISM ARRAY FOR LARGE-SCALE, WIDE-BAND INTERCONNECTION OF OPTOELECTRONIC SYSTEMS

Final Report

March 15, 1992

Contract No. DAAL03-91-C-0030


Period of Performance: 07-01-91 to 12-31-91

Sponsor:

U.S. Army Research Office
P. O. Box 12211
Research Triangle Park, NC 27709-2211

Contractor:

Physical Optics Corporation
20600 Gramercy Place, Suite 103
Torrance, CA 90501
(310) 320-3088

92-11477


Author/Principal Investigator:

Ray T. Chen, Ph.D.
(310) 530-1416

92 4 28 09 6

ABSTRACT

Microprisms and microprism arrays have been proposed and then successfully demonstrated for two-dimensional (2-D) and three-dimensional wide-band optoelectronic interconnects. Microprisms with linear dimensions from $\sim 100\ \mu\text{m}$ to $\sim 1\ \text{mm}$ were fabricated using fiber-drawing and plate-cutting methods. 2-D optical interconnects using microprisms as the input and output couplers in conjunction with an optical bus were demonstrated. Ten parallel channels were simultaneously provided by using a 670 nm laser diode array. Coupling efficiency as high as 81% was experimentally confirmed. The measured 3 dB bandwidth using a microprism for free space to optical bus coupling was measured to be 250 nm (710 nm to 960 nm). The coherent pace of the material dispersion for the microprism and the optical bus explains the ultrawide coupling bandwidth which is around 2 orders of magnitude higher than that of holographic optical elements (HOEs).

A 3-D board-to-board optical interconnect with 60 GHz bandwidth (microwave) and 22 dB signal-to-noise ratio (equivalent to a bit error rate of 10^{-10}) was realized using four microprism couplers.

Finally, due to the innovativeness, the practicality and the cost effectiveness of the proposed concept, a myriad of feasible applications present themselves. These include clock signal distribution multi-wafer optical interconnects for 3-D multi-processor computers, optical sensing probes, phased array antennas, and plasmon resonant devices.

Accession For	
NTIS CRA&I	<input checked="" type="checkbox"/>
DTIC TAB	<input type="checkbox"/>
Unannounced	<input type="checkbox"/>
Justification	
By	
Distribution /	
Availability Codes	
Dist	Avail and/or Special
A-1	

IN 3

TABLE OF CONTENTS

ABSTRACT	ii
LIST OF FIGURES	iv
LIST OF TABLES	iv
1.0 SUMMARY	1
2.0 WAVELENGTH DISPERSION OF THE MICROPRISM AND THE OPTICAL DATA BUS (ODB)	2
2.1 The Need to Use Microprisms	4
3.0 MICROPRISM FABRICATION.....	5
4.0 DEMONSTRATION OF 2-D OPTICAL INTERCONNECTS.....	9
5.0 FURTHER APPLICATIONS	17
5.1 Clock Signal Distribution	17
5.2 Multiwafer Scale Integration for Ultrafast 3-D Optical Computers	18
5.3 Miniaturized Sensor Probe.....	20
5.4 Optically-Controlled Phased Array Antennas.....	22
5.5 Surface Plasmon Resonant Device Using a Microprism	22
6.0 CONCLUSION	25
7.0 REFERENCES	27

LIST OF FIGURES AND TABLES

Figure 1	Interconnection Hierarchy	3
Figure 2	Side View of Optical Wave Coupling From Microprism to Optical Data Bus	3
Figure 3	Spot Sizes of a Guided Wave From an Optical Data Bus Coupled Out by a Microprism ($\sim 100 \mu\text{m}$) and a Conventional Prism (3 mm to 1 cm). 5	
Figure 4	Microprism Design Parameters. The material LaSF9, $n_{632.8} = 1.845$. The shapes shown are cross sections.	6
Figure 5	Schematic of a Microprism Fiber Drawing System ^[9]	7
Figure 6	MPC Fabrication Using Iteration of Plate Alignment, Cutting and Polishing.....	8
Figure 7	MPC/ODB Integration Using 70° - 55° - 55° Prism.....	8
Figure 8	Fabricated Microprisms with Cross Sections Equivalent to (a) Figure 4(a), (b) Figure 4(b), (c) Figure 4(c), and (d) Figure 4(d)	9
Figure 9	Schematic of the Phase-Matching Condition for Microprism-to-Optical Bus Coupling.....	10
Figure 10	Ten Channel Parallel Coupling with (a) an Input Microprism Coupler, and (b) an Input and Output Microprism Coupler.....	10
Figure 11	Measured Output Power of Each Channel	11
Figure 12	Experimental Setup for Coupling Bandwidth Measurement.....	11
Figure 13	Measured Coupling Bandwidth of Microprism to Optical Bus Power Transfer	12
Figure 14	(a) Photograph of Board-to-Board Optical Interconnection Using Polymer-Based Optical Data Boards in Conjunction with Microprisms, and (b) Schematic of Figure 14(a). The coupling stages are not shown.....	14
Figure 15	Near-Field Images of (a) TEM ₀₀ Laser Light at Location 1 (Figure 1(b)), (b) Mode Dot at Location 2, and (c) Mode Dot at Location 4. .	15
Figure 16	Generation, Transmission, and Detection of 60 GHz Signal for 55 cm Board-to-Board Optical Interconnection.	16
Figure 17	60 GHz Signal Detected at Location 4 (Figure 14(b)). A 22 dB signal-to-noise ratio is clearly indicated.	17
Figure 18	Clock Signal Distribution Using the Combination of MPC and Multiplexed HOE.	18
Figure 19	Multiwafer Scale Integration for Ultra-Fast 3-D Optical Computer Using MPC as the Interconnection Tool	19
Figure 20	Vertical Coupling Using Microprism in Conjunction with Optical Bus	19
Figure 21	Microprism for Free Space-to-Optical Bus Coupling (Board 5 of Figure 19)	20
Figure 22	Fiber Optic Sensor Technology Availability.....	21
Figure 23	Microprism-based Miniaturized Sensor Probe	22
Figure 24	High Density Phase-Delay Lines Using Microprism Arrays in Conjunction with Integrated Optical Circuits	23
Figure 25	Surface Plasmon Resonant Device Based on Microprism	23
Figure 26	SPP Coupling to Evanescent Waves, with Free-Space Dispersion ω_D , Surface Plasmon Cutoff ω_{SP} and SPP Dispersion Curve ω_{SPP} . Dotted lines show the coupling condition.....	24
Figure 27	Measured Response of SPR as a Function of Incident Angle ($\lambda = 632.8 \text{ nm}$)	25
Figure 28	Demonstrated Modulation Bandwidth of Board-to-Board 3-D Optical Interconnects	26
Table 1	Demonstrated Features of Microprism with HOEs as a Reference.....	2

1.0

SUMMARY

The need for higher throughput, greater connectivity and resistance to electromagnetic and radio frequency interference in the areas of computer interconnects, networking, communications, and sensors calls for replacement and hybridization of the present-day electronic components with optical and optoelectronic devices. One-dimensional and two-dimensional modulator arrays [1,2], high density optical memory devices [3] and high-speed optical data buses [4,5] are some of the most important technologies where optoelectronic devices [8,9] can replace existing devices. One of the major unsolved problems in realizing a high-speed, highly-parallel optoelectronic system is the lack of appropriate microstructure optical components to interface the various discrete optical components. Recently, optical interconnects using the combination of lasers, waveguides (fiber and integrated optics) and holographic optical elements (HOEs) were proposed [6,7] and then developed. Routing of an optical signal from site-to-site through these components is intrinsically narrow-band because of the stringent requirement of the phase matching condition for the diffraction HOE.

In this program, Physical Optics Corporation (POC) proposed and then successfully developed a wide-band micropism coupler. Micropism design and fabrication were accomplished first. The coupling bandwidth was experimentally determined. A coupling bandwidth of 250 nm from free space to the single-mode optical bus was demonstrated. Wavelength dispersion of both the micropism and the optical bus was considered. The extra large coupling bandwidth is due to the coherent pace of the dispersion relation of these two material systems.

Demonstration of 2-D and 3-D optical interconnects, including a 30 cm intraboard interconnect and 60 cm board-to-board interconnect also took place in this program. The bandwidths of these demonstrations are as high as 60 GHz, while the signal-to-noise ratio is 22 dB, corresponding to a bit error rate (BER) of 10^{-10} . The major achievements of the Phase I program are summarized in Table 1, with the HOEs as a reference. Micropisms outperform HOEs in features 1, 3, 4, 5, 8, and 9. Three-dimensional (3-D) interconnects represent the most serious bottleneck of current high performance computers since they are longer. The interconnection hierarchy of all existing interconnect schemes is shown in Figure 1. Machine-to-machine interconnects are largely optical fibers. Three-dimensional interconnects involving board-to-board and module-to-module interconnection are the major impediments for highly parallel multi-processor computers. The achievement of a 60 GHz wide-band 3-D optical interconnect with 22 dB signal-to-noise ratio using micropism in conjunction with optical data bus (further information is presented in Section 5.0) detailed in this report represents the most successful result demonstrated so far. Advantages such as high coupling efficiency (3), cost effectiveness (4) and mass producibility (5) are also important factors with which the HOE counterparts cannot compete. Applications of the proposed technology include clock signal distribution for synchronous buses, multiwafer scale integration for ultrafast fine-grained computers, optical backplanes, optical sensor probes, phased array antennae and surface plasmon resonant devices.

Table 1. Demonstrated Features of Microprism with HOEs as a Reference

Feature	Microprisms	HOEs
1. Coupling Bandwidth	250 nm	<10 nm
2. Size	to 100 μm^a	to 100 μm^a
3. Efficiency	82% ^b	70% ^c
4. Cost	Low ^d	High ^d
5. Mass Producibility	Yes	No ^e
6. Substrate Transferability	Yes	Yes
7. 2-D Interconnect	Yes ^f	Yes ^f
8. 3-D Interconnect	Yes	Not Practical ^g
9. Demonstrated Microwave Bandwidth	60 GHz/22 dB signal-to-noise ratio	500 MHz

a Size can be even smaller; however, smaller than 100 μm may not be useful.

b Theoretically it is 87% [10]. In Phase I, we demonstrated 82% efficiency.

c Theoretically it can go as high as 90 - 100%. The experimental results were ~70%.

d Microprisms made by fiber-drawing can cost as low as 10¢/piece while high-efficiency volume HOEs are high in cost (~\$10/piece in large quantities).

e Thin hologram with low diffraction efficiency can be made with embossing technology. High efficiency HOEs are made piece by piece through direct laser beam recording.

f Both are useful for 2-D interconnects. For a large fan-out number, multiplexed HOEs will be the device of choice.

g This is the most important drawback of HOE-based optical interconnects; they are intrinsically narrow-band (<10 nm). On the other hand, microprisms have a demonstrated 3-D coupling bandwidth of 250 nm (feature 4), the highest ever demonstrated.

2.0 WAVELENGTH DISPERSION OF THE MICROPRISM AND THE OPTICAL DATA BUS (ODB)

To efficiently couple wide-band optical signals into and out of an optical data bus (ODB) through a microprism (Figure 2), a phase matching condition must be satisfied, i.e.,

$$N_p \cos \theta_1 = N_g \cdot \cos \theta_2 \quad (1)$$

where N_p and N_g are the refractive indices of the prism and waveguide, respectively, and θ_1 and θ_2 are as indicated in Figure 2. Note that $N_g \cdot \cos \theta_2$ is the effective index (N_{eff}) of the ODB. The angle θ_1 can be represented as

$$\theta_1 = \frac{\pi}{2} - \varphi + \delta \quad (2)$$

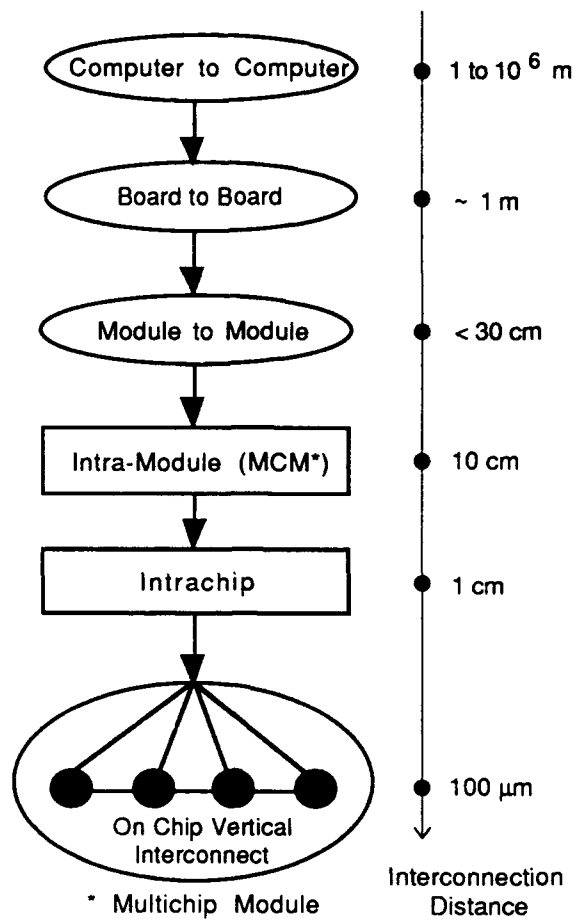


Figure 1
Interconnection Hierarchy

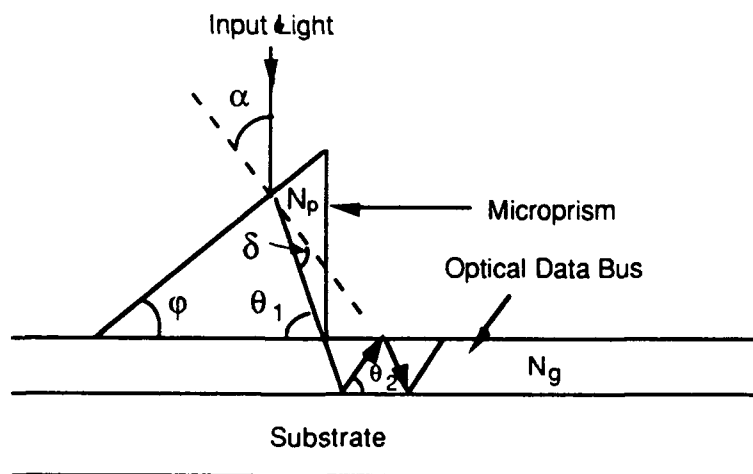


Figure 2
Side View of Optical Wave Coupling From Microprism to Optical Data Bus

In Eq. (2) ϕ and δ are the prism angle and the prism deflection angle (Figure 2), respectively. A wide coupling bandwidth from the prism to the optical data bus (ODB) means that, for a fixed angle δ and thus α , an optical beam with a large optical bandwidth can be coupled into and out of the ODB. Based on Eqs. (1) and (2), a wide-band microprism coupler (MPC) shall have

$$\left. \frac{dN_{\text{eff}}}{d\lambda} \right|_{\lambda_1 < \lambda < \lambda_2} = \left. \frac{d(N_p \cos \theta_1)}{d\lambda} \right|_{\lambda_1 < \lambda < \lambda_2} = \left. \frac{d(N_g \cos \theta_2)}{d\lambda} \right|_{\lambda_1 < \lambda < \lambda_2} \quad (3)$$

(λ_1, λ_2) is the wavelength interval to be coupled. Eq. (3) is valid for both 2-D and 3-D optical interconnects involving microprisms. Eq. (3) implies

$$\frac{dN_{\text{eff}}}{d\lambda} = A \cdot \frac{dN_p}{d\lambda} = B \cdot \frac{dN_g}{d\lambda} \quad (4)$$

where $A = \cos \theta_1 + \sin \theta_1 (d\theta_1 / dN_p)$ and

$$B = \sin \left[\left(\phi - \sin^{-1} \left(\frac{\sin \alpha}{N_p} \right) \right) + N_p \cos \left(\phi - \sin^{-1} \left(\frac{\sin \alpha}{N_p} \right) \right) \right. \\ \left. \left(\sin^{-1} \left(\frac{\sin^{-1} \alpha}{N_p} \right) \right) \cdot \frac{N_p^2}{\sqrt{1 - \frac{\sin \alpha}{N_p}}} \sin \alpha \right] \quad (5)$$

All of the physical parameters involved in Eq. (5) can be found in Figure 2. Eq. (4) is the criterion needed to provide a wide-band MPC. Generally speaking, optical material maintains the behavior of its dispersion relation when the optical wavelength shifts. This statement is correct except in the anomalous dispersion region [9]. The exact value of A and B can be determined from experimental data. The optimization of the material combination will provide us with an MPC optical data bus for large-scale optoelectronic integrated systems. One of the Phase I major tasks was to determine the values of A and B for different materials. The 250 nm bandwidth (with a fixed α angle) was demonstrated with the combination of LaSF9 glass and the optical data bus. Note that the size of the detector for a prism-based 3-D interconnection can be much smaller than for a HOE-based interconnection due to the fixed α angle. As a result, a higher speed detector can be implemented on the receiver [8].

2.1 The Need to Use Microprisms

Although prism couplers can provide wider coupling bandwidths, a conventional prism coupler still cannot efficiently couple light from waveguide to fiber or from waveguide to waveguide. The in-plane scattering and Gaussian beam divergence enlarge the prism-coupled spot size (either m-dot or m-line) in the direction perpendicular to the guided wave propagating direction. The larger the prism, the larger the spot size. Figure 3 shows the schematic of the spot sizes coupled out from (a) a microprism and (b) a conventional prism.

The diameter of the spot coupled out by the microprism is compatible with multi-mode fibers (50/125, 62.5/125, 100/140 μm). The spot size out of the conventional prism is too large to be matched with a multi-mode fiber. The innovative method we propose provides an easy and feasible way to solve this interface problem. The success of this project will have a significant impact on networking for phased array antennas where both optical fibers and single-mode integrated optical devices are involved. Furthermore, the real-estate of optoelectronic surfaces is heavily occupied by VLSI circuits including logic gates, data buses, memory chips, etc. Implementation of the wide-band MPCs is the only method to provide board-to-board (3-D) and intraboard (2-D) interconnects. Note that the interface problem between multi-mode fibers and the single-mode ODB has not been solved to date. The idea shown in Figure 3 provides a feasible solution.

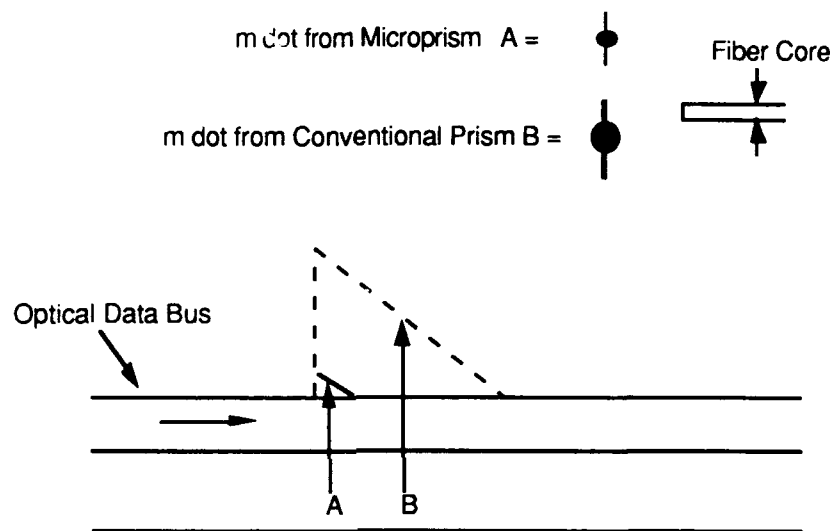


Figure 3
Spot Sizes of a Guided Wave From an Optical Data Bus Coupled Out by a Microprism
($\sim 100 \mu\text{m}$) and a Conventional Prism (3 mm to 1 cm)

3.0 MICROPRISM FABRICATION

The ultimate goal of this program is to demonstrate a microprism-based optical interconnection network suitable for a large-scale optoelectronic system. The physical parameters of the microprisms are summarized in Figure 4.

The most important parameter is ϵ since it determines the input and output coupling angles for board-to-board and module-to-module optical interconnections. Although much smaller prisms can be made, the physical sizes of these prisms are fixed in the neighborhood of 1 mm. The microprisms introduced in this program will be a key element for board-to-board and module-to-module optical interconnects (Figure 1).

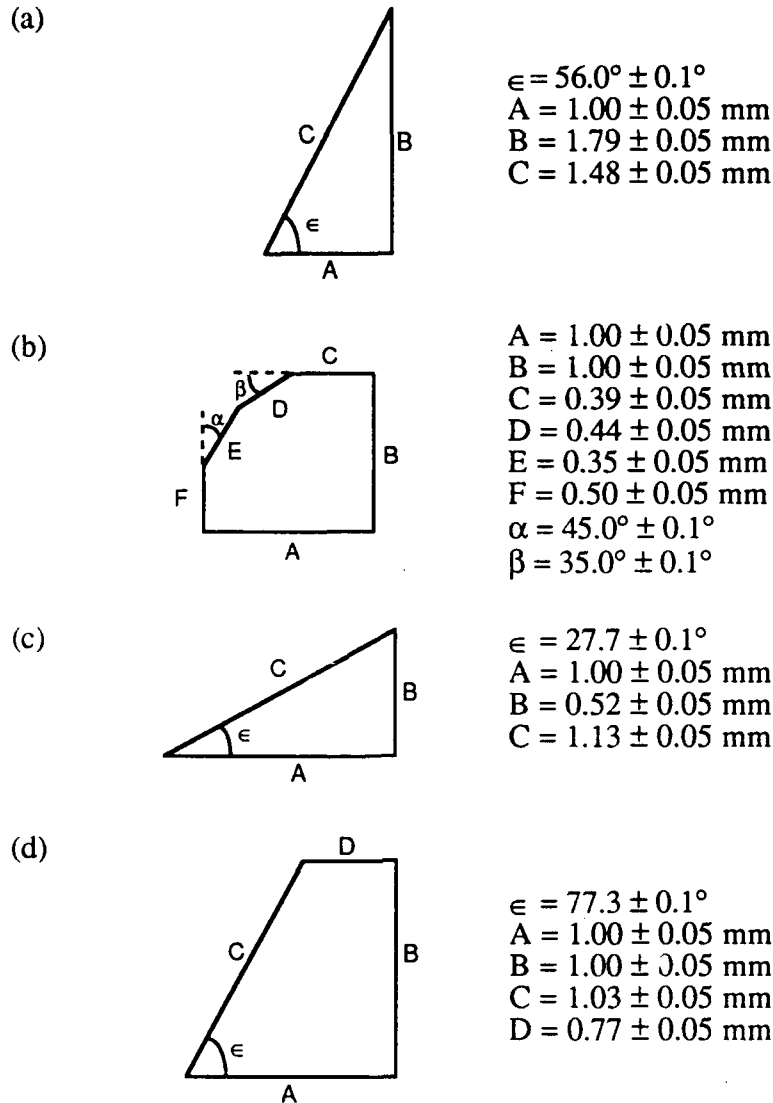


Figure 4
Microprism Design Parameters. The material is LaSF9, $n_{632.8} = 1.845$.
The shapes shown are cross sections.

There are two ways to produce the MPCs. They are (1) prism fiber drawing and (2) plate cutting and polishing. Microprism fibers are made by first preparing a glass blank, or preform, which has the shape of the microprism desired. Once the preform has been developed, the microprism fiber is drawn from the preform. The elements of a typical drawing tower are shown in Figure 5. The preform is placed in a furnace where the tip is heated to $2100^\circ - 2200^\circ\text{C}$. A capstan pulling apparatus is used to pull or draw the fiber into a specified diameter. While the microprism fiber is drawn, the size of the prism is controlled by the drawing speed. The size of the microprism fiber is monitored during the drawing process by a laser gauge. The fiber drawing process impacts the optical characteristics, dimensions and strength of the fiber. The optical properties are affected by the atomic absorption in the glass structure, contaminants that become trapped in the fiber

during the drawing process, density fluctuation of the glass, and microbending loss due to improper coating design [9] and application. Cleanliness during the process is very important.

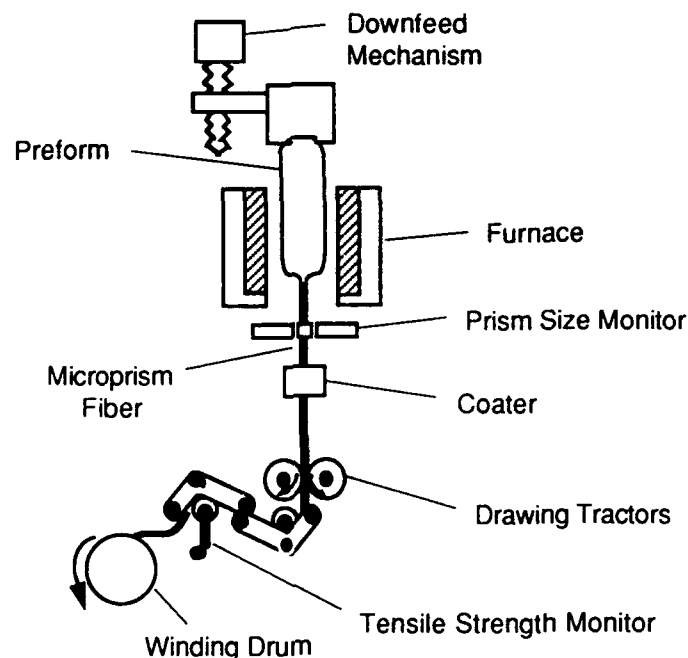


Figure 5
Schematic of a Microprism Fiber Drawing System [9]

The three faces of the MPC are precisely controlled (to a few μm accuracy) during the fabrication process. The length of the prism is determined by final cutting after the formation of the microprism fiber.

The second method of fabrication is by plate cutting and polishing. The process of fabrication is straightforward. After stacking a number of glass plates with the desired thickness, iteration of alignment, followed by cutting and polishing procedures will result in MPCs with the desired geometry. Figure 6 shows the process of fabrication.

Microprism fiber drawing is appropriate for mass production, while plate cutting and polishing is good for small quantity prototype demonstration. It is expected that by the end of Phase II, POC will have the mass production capability to generate the proposed devices for both the civilian and military markets. Figure 7 shows MPC/ODB integration using a $70^\circ\text{-}55^\circ\text{-}55^\circ$ microprism. The prism shown in Figure 7 was generated through plate cutting and polishing. A small number of microprisms can be produced with this method. For large quantity fabrication, microprism fiber drawing is more realistic. The microprisms shown in Figure 4 were fabricated by fiber drawing. The cross section of the microprism was controlled by the winding speed of the fiber drawing setup (Figure 5). The desired dimension of the fiber prism was achieved by cleaving the prism fiber. Figure 8 displays the cross sections of three-microprisms with the dimensions described in Figure 4.

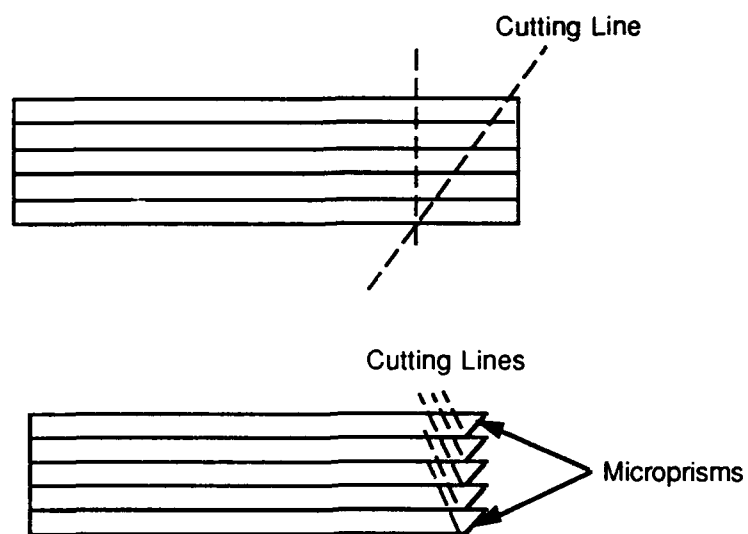


Figure 6
MPC Fabrication Using Iteration of Plate Alignment, Cutting and Polishing



Figure 7
MPC/ODB Integration Using 70°-55°-55° Prism

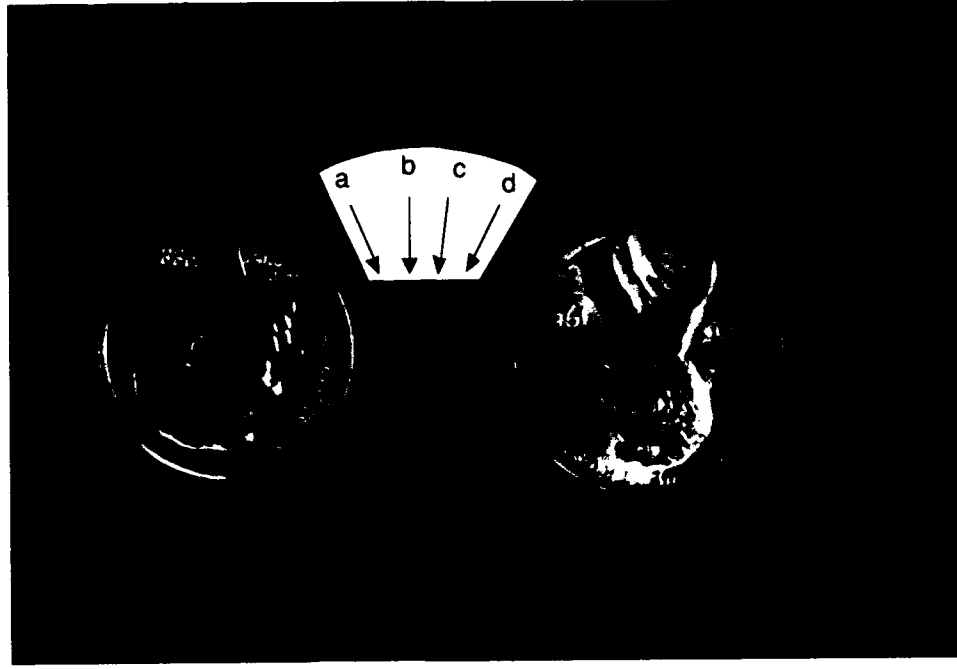


Figure 8
Fabricated Microprisms with Cross Sections Equivalent to
(a) Figure 4(a), (b) Figure 4(b), (c) Figure 4(c), and (d) Figure 4(d)

4.0 DEMONSTRATION OF 2-D OPTICAL INTERCONNECTS

The first interconnection experiment which we performed was a 2-D optical interconnect involving two microprisms and one polymer-based optical bus. Microprisms with linear dimensions from 1 mm to 40 mm were used for this purpose. In a prism coupler, the incoming laser beam is totally reflected at the base of the prism and the lightwave in the prism is coupled into the optical bus, i.e., waveguide, through the evanescent fields. The direction of the laser beam in the prism must be such that the synchronous condition (Eq. (1)) indicated by the vector diagram shown at the right of Figure 9 is satisfied. The maximum coupling efficiency can be achieved when

$$\frac{1}{2} - \ell |T|^2 / 2t \tan \theta_1 = 1.25 \quad (6)$$

where ℓ is the coupling length (Figure 9), t is the waist of the Gaussian beam, θ , is the prism coupling angle (Figure 2) and

$$T \cdot T^* = e^{-2kd} \sin 2\phi_1 \sin 2\phi_2 \quad (7)$$

In Eq. (7), ϕ_1 and ϕ_2 are the Fresnel phase shifts at the film-air and prism-air interfaces, k is the decay term of the waveguide mode in the air/optical bus interface, and d is the air gap between the microprism and the optical bus (see Figure 9). It is clear from Eq. (7) that the value of d plays an important role in maximizing the coupling efficiency. Conventionally, a

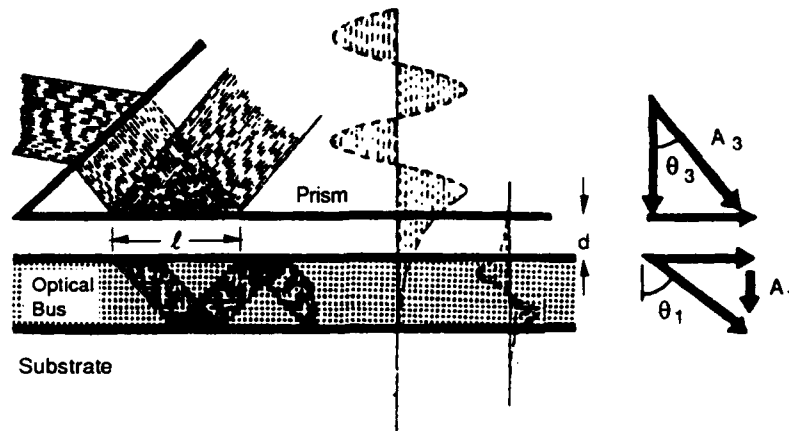


Figure 9
Schematic of the Phase-Matching Condition for Microprism-to-Optical Bus Coupling

prism clamp was employed to minimize the air gap. Experimentally, coupling efficiency as high as 88% was reported by Ulrich [10] in 1970. An important feature we have demonstrated in Phase I is the attachment of the microprism to the optical bus through van der Waals force. Since the microprism is so small, and thus light in weight, the two optical elements, i.e., microprism and optical bus, can be joined together without the external binding force needed for the conventional microprism. This greatly enhances the integration of systems involving many processing nodes. The experimental results for 10 parallel channel interconnections are displayed in Figure 10. Free space-to-optical bus coupling using an input microprism coupler is shown in Figure 10(a). Ten optical bus channels are evenly distributed. The separation of each channel is 2 mm, chosen to provide visual clarity. Microprisms can be used for coupling not only into the optical bus but also out of the optical bus. Figure 10(b) demonstrates both schemes. The optical guided waves can be coupled in and out uniformly, as indicated by the photograph.

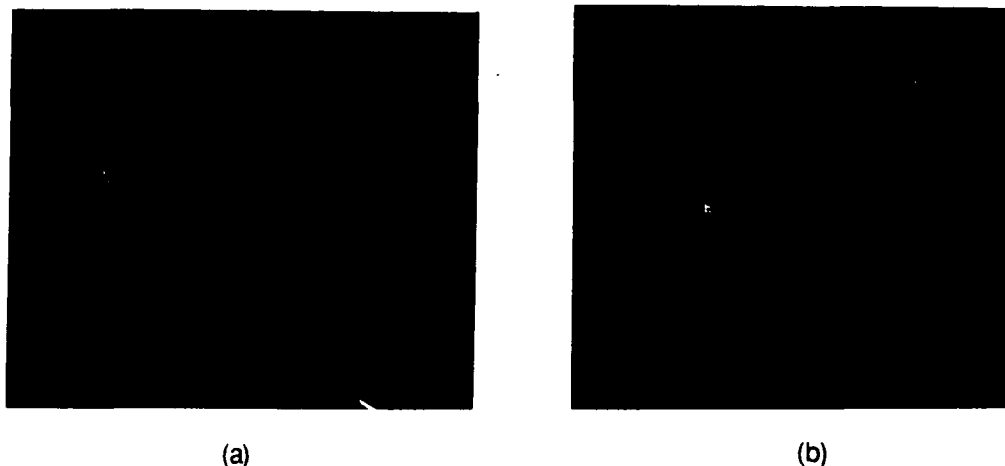


Figure 10
Ten Channel Parallel Coupling with (a) an Input Microprism Coupler, and (b) an Input and Output Microprism Coupler

The optical power coupled out from each channel was measured and the data is illustrated in Figure 11. The maximum output power difference is within 5% over all 10 channels. The uniformity of the output power represents an unvarying air gap, d , all over the coupling area. The coupling efficiency for a single channel was further measured using a tunable Ti-sapphire laser. The measurement setup is shown in Figure 12 in which the optical bus coupling stage, Argon laser (pumping source), Ti-sapphire laser, collimator, vidicon camera, TV monitor, and power meter are clearly shown. The measured result is delineated in Figure 13. Coupling efficiency as high as 81% is observed and the 3 dB coupling bandwidth is more than 250 nm. Note that the output coupling efficiency (optical bus-to-free space) of 100% can be easily achieved. The result outperforms hologram-based 3-D coupling, which has a typical bandwidth of less than 10 nm.

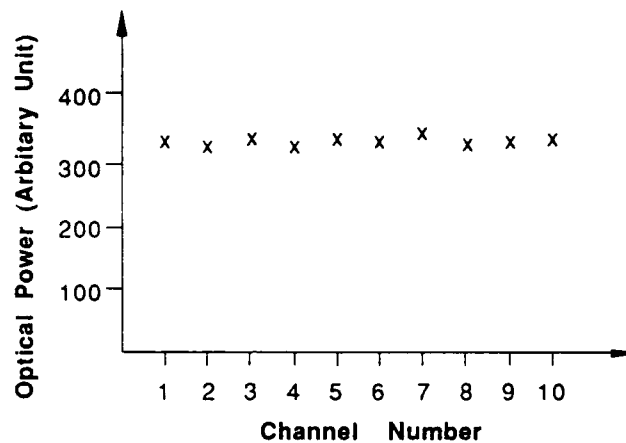


Figure 11
Measured Output Power of Each Channel

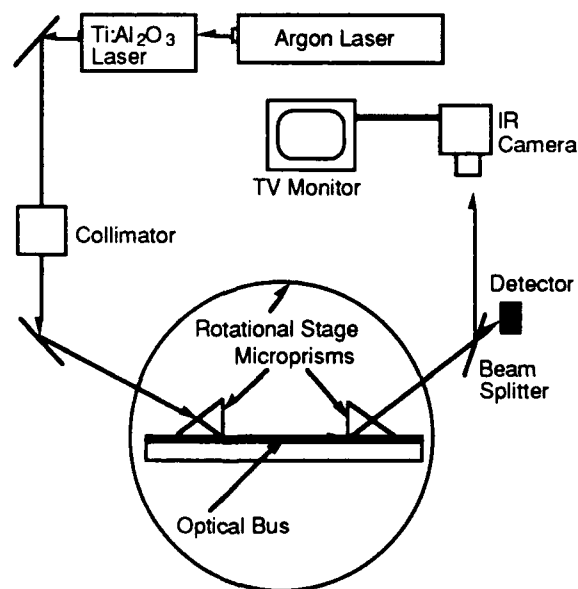


Figure 12
Experimental Setup for Coupling Bandwidth Measurement

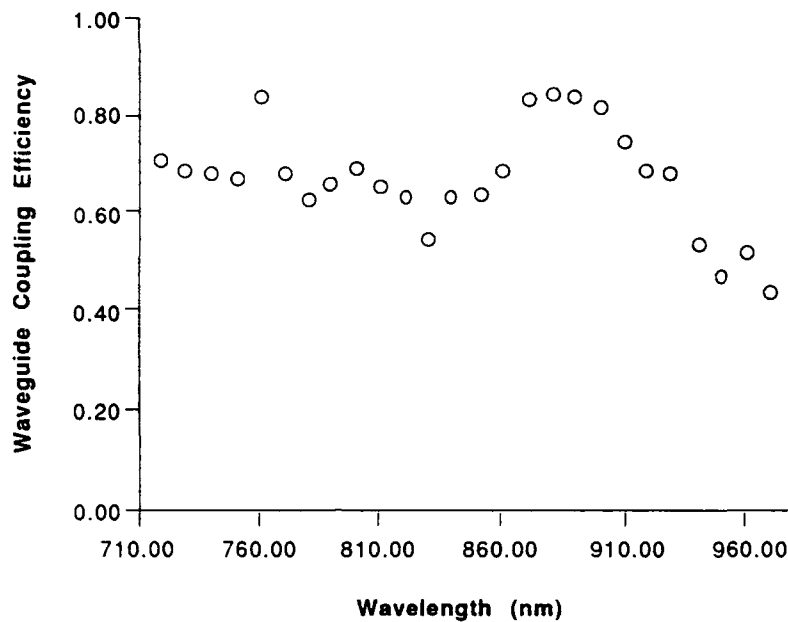


Figure 13
Measured Coupling Bandwidth of Microprism to Optical Bus Power Transfer

We achieved a 60 GHz board-to-board optical interconnection using polymer optical buses in conjunction with microprism couplers. An intra-board interconnection distance as long as 30 cm was previously demonstrated [11]. The result demonstrated in this project employs two optical bus boards containing a graded index (GRIN) polymer waveguide [12]. Board-to-board interconnection was realized using microprism couplers made out of LaSF glass. The current performance of state-of-the-art electronic systems, especially large computers, is limited by electrical interconnects rather than the on-chip processing speed. As the number of components per chip and the processing speed increase drastically, electrical interconnection becomes inadequate on module-to-module and board-to-board levels [13]. A multi-chip module (MCM) for a high speed, highly parallel electronic system (e.g., IBM's System/390 mainframe uses an MCM that holds 121 chips, spaced about 3/8 inch apart) was implemented to minimize the speed limitation imposed on electrical interconnections (EI). However, the intrinsic characteristics of conventional electrical interconnections prohibit transmitting a 1 GHz signal farther than 1 mm [14]. The use of transmission lines involves ground plane implementation, becomes dispersive, and results in significant losses from the skin effect as the speed increases.

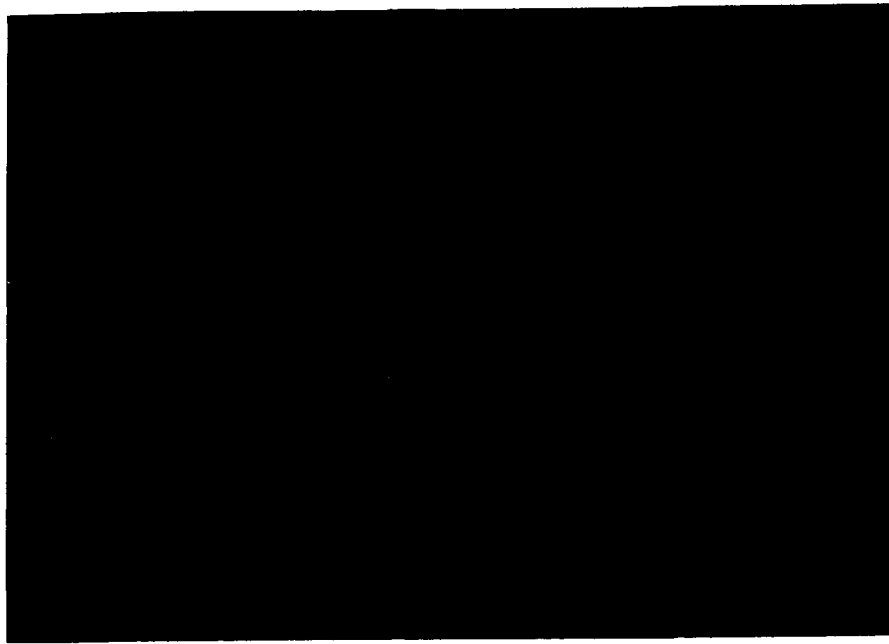
In this section, the demonstration of 60 GHz board-to-board optical interconnections with distances as long as 55 cm is presented. The demonstration used single-mode graded index (GRIN) polymer waveguides in conjunction with microprisms. The high speed optical signal was generated by coherently mixing two lasers: $\psi_1 = A \cos \omega_1 t$ and $\psi_2 = B \cos \omega_2 t$.

At the receiving end, the demodulation process involves a square law detector which displays the intensity of the optical signal. That is [15]

$$I = \frac{e\eta}{\hbar\omega} \left[A^2 + B^2 + 2C(\omega_{\text{beat}}) \cdot \cos\phi \cdot AB \cos(\omega_{\text{beat}}t) \right] \quad (8)$$

where $\omega_{\text{beat}} = \omega_1 - \omega_2$, e is the electron charge, η is the quantum efficiency, $\hbar\omega$ is the photon energy, $C(\omega_{\text{beat}})$ is the frequency response of the detector and ϕ is the angle between the polarized directions of the two light waves. The frequency of the beat signal is controlled by the frequency separation of the two lasers. By coherently mixing ψ_1 and ψ_2 , the detected signal represented by Eq. (8) contains a combination of the DC part and a modulated part. The result represented by Eq. (8) is equivalent to that of an optical wave, modulated at a microwave frequency ω_{beat} . The two lasers we employed were a Kition red dye laser (600 nm to 640 nm, 400 mW) and a frequency stabilized HeNe laser (632.8 nm, 0.6 mW). The wavelength of the dye laser was locked to an external-temperature-stabilized Fabry-Perot reference cavity. The linewidth and stability of both lasers was typically less than 2 MHz. Propagation of the mixed optical waves from input port to output port is illustrated in Figure 14(a). A schematic representation of Figure 14(a) is depicted in Figure 14(b). The coupling stages are not shown in Figure 14(b). Due to the GRIN property of the polymer thin film [11,12], the optical bus boards can be made out of any substrate of interest, such as Al_2O_3 , Si, GaAs, glass, or PC board. Our demonstration was done using BK-7 glass substrates. The measured optical insertion loss from location 1 to location 4 (Figure 14) was ~ 6 dB (excluding Fresnel reflection). The input TEM_{00} mode (location 1) and the m-dots coupled out at locations 2 and 4 are shown in Figures 15(a), (b), and (c), respectively. Formation of the well defined m-dots verified the quality of the polymer waveguide. The in-plane scattering of the optical bus board was very small. The polymer waveguide implemented has a wide optical transmission bandwidth from ~ 300 nm to ~ 2800 nm [12]. As a result, intra-board optical interconnections using ultraviolet, visible, and near infrared wavelengths as the signal carrier can be realized.

The experimental setup for the high speed board-to-board optical interconnection is shown in Figure 16, where the coherently mixed optical signal is collinearly coupled into the first optical bus board through a prism coupler. The optical bus board is adjusted such that the tangential components of the electromagnetic fields are continuous at the prism/gap/waveguide interface to generate "optical tunneling". The optical beam containing the ω_{beat} (Eq. (8)) propagates across the first optical bus board and then couples out of the first board using another prism coupler. To efficiently couple the optical wave from the first optical data board to the second one, control of the profile of the beam coupled out from the output prism coupler of the first optical data board is extremely important. A good quality optical waveguide and an appropriate prism-to-waveguide attachment provided us with an output beam with well defined m-dots (Figure 15(b)) which facilitated the coupling into the second optical bus board. By employing a similar technique, a good quality m-dot was coupled out of the second optical data board (Figure 15(c)). The optical "signal" coupled out of the second optical bus board was focused onto the detector using an 10x objective lens. The demodulation scheme is shown in Figure 16. The detector is a three stage amplifier circuit consisting of a discrete AlGaAs/InGaAs high electron mobility transistor (HEMT) [16] in series with a two stage 60 GHz millimeter-wave monolithic integrated circuit (MMIC) amplifier [17]. The optical mixing takes place in the active region of the discrete HEMT device. The 60 GHz output was amplified by the MMIC and fed into waveguide via a microstrip to coaxial to waveguide transition. The signal was then downconverted to intermediate frequencies (1-2 GHz) using a directional coupler fed local oscillator (Klystron) and a waveguide mixer. In the initial phases of this experiment,



(a)

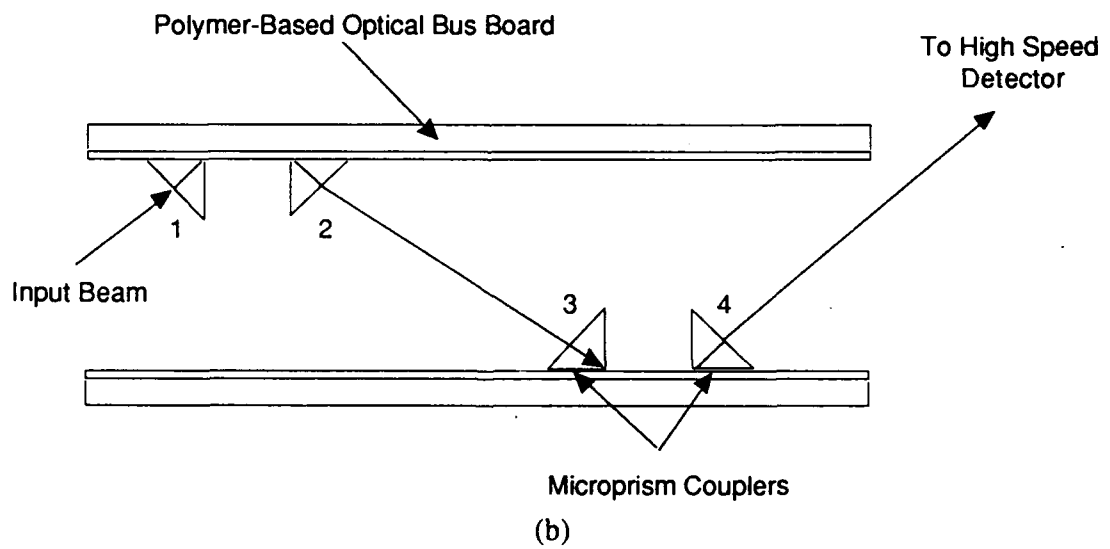


Figure 14

(a) Photograph of Board-to-Board Optical Interconnection Using Polymer-Based Optical Data Boards in Conjunction with Microprisms, and (b) Schematic of Figure 14(a). The coupling stages are not shown.

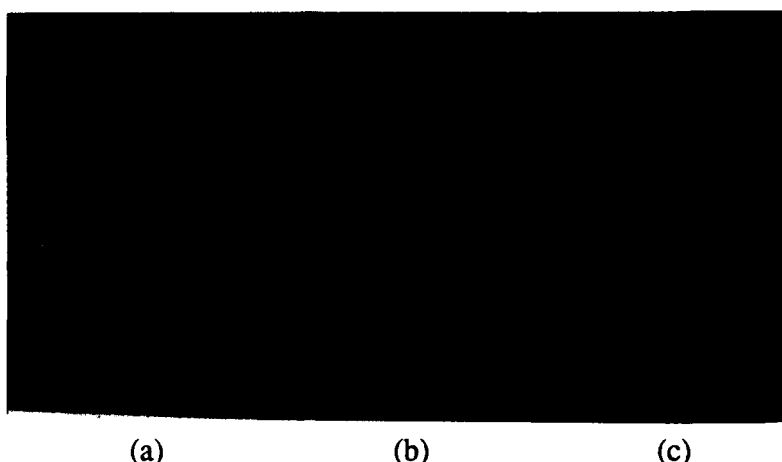


Figure 15
Near-Field Images of (a) TEM₀₀ Laser Light at Location 1 (Figure 1(b)), (b) Mode Dot at Location 2, and (c) Mode Dot at Location 4.

continuous tuning of ω_{beat} from 1 GHz to 25 GHz was demonstrated to establish the large bandwidth capability of this system. We then switched to the highest frequency of our new detection system and the result shown in Figure 17 is the heterodyne detected signal at 60 GHz. As previously mentioned, the beat signal represented by Eq. (8) is equivalent to a modulated base band signal using a high speed laser diode or an external modulator driven by a single frequency microwave source. The availability of a high speed transceiver will allow us to demonstrate board-to-board optical interconnections with fully on-board modulation and demodulation capabilities [8,19]. A GRIN polymer waveguide lens [20] can also be used to provide a diffraction-limited spot and thus achieve high speed signal detection.

The experimental results demonstrated in this project conclude that the GRIN polymer waveguide can be used as a high speed optical bus for board-to-board optical interconnection with speeds as high as 60 GHz and bit error rates (BER) of 10^{-10} (22 dB signal-to-noise ratio). It should be noted that the limit on speed was imposed by the system power budget rather than the polymer-based optical bus board. A 1 GHz board-to-board optical interconnection through free space was previously demonstrated [21]. Here a 60 GHz board-to-board optical interconnection involving a single-mode polymer waveguide is reported for the first time. For the three-dimensional (3-D) optical interconnection demonstrated in this program, board-to-board interconnections were realized through free space rather than an optical backplane [22]. Optical interconnections through a backplane introduce an extra degree of material dispersion and thus impose a more stringent speed limit for 3-D optical interconnections. 3-D optical interconnections using holographic optical elements (HOEs) turn out to be impractical [13] due to the required phase-matching condition associated with them. Such coupling devices are intrinsically narrow-band, which strictly limits the availability of light sources. To cover the required interconnection distances using HOEs while still maintaining a good power budget, the entire area of the detector has to be enlarged to compensate for the deviation of

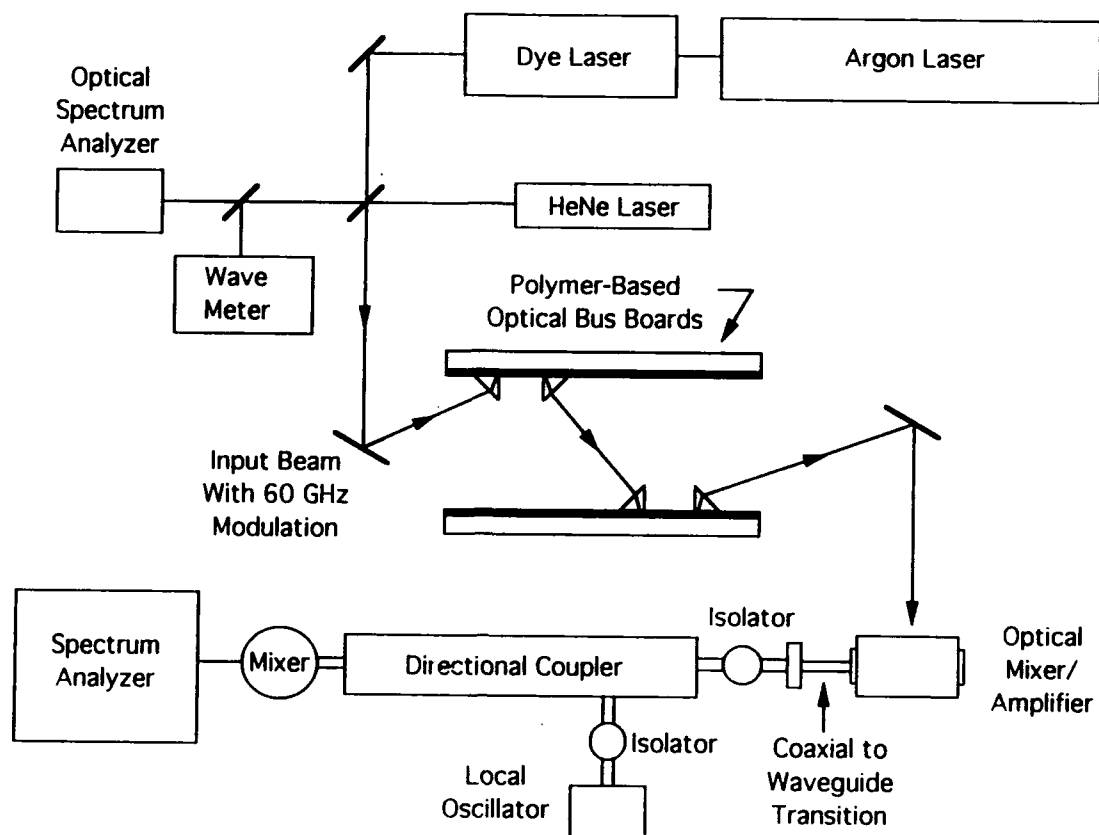


Figure 16
Generation, Transmission, and Detection of 60 GHz Signal for 55 cm Board-to-Board Optical Interconnection

the optical beam propagation due to the shift of the optical wavelength. Consequently, the speed of 3-D optical interconnections involving HOEs will be significantly reduced. On the other hand, the microprism we employed is a wide-band coupler. By fixing the input beam at the coupling angle which is phase-matched to the effective index of the guided wave, a 3 dB coupling bandwidth of more than 250 nm was experimentally confirmed using a Ti-Sapphire laser.

The beat signal, which was 60 GHz in our demonstration, is similar to an optical signal modulated by either an external modulator or a laser diode using a 60 GHz single frequency microwave as the modulation source. Implementation of transmitter and receiver onto the optical data board will allow us to demonstrate a fully on-board optical interconnection scheme involving modulation and demodulation processes. Implementation of a polymer waveguide lens onto the optical data board will provide us with a diffraction-limited spot and thus ease the demodulation criterion. The reported speed limit is due to the system power budget rather than the GRIN polymer waveguide. Finally, the combination of a GRIN polymer waveguide and a LaSF microprism provided us with a 250 nm free space to optical data board coupling bandwidth, which is two orders of magnitude higher than for an HOE.

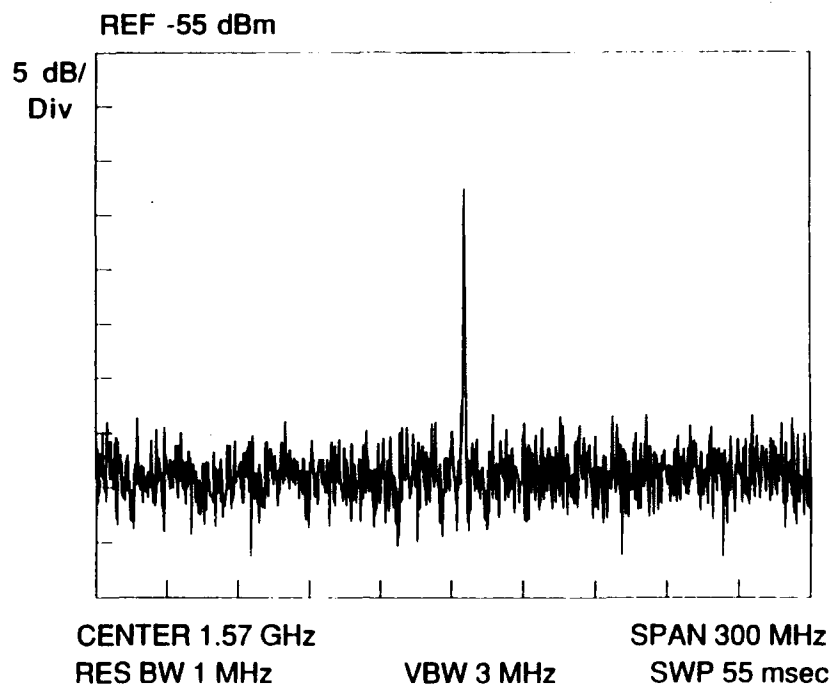


Figure 17
60 GHz Signal Detected at Location 4 (Figure 14(b)). A 22 dB signal-to-noise ratio is clearly indicated.

5.0 FURTHER APPLICATIONS

Microprisms and microprism arrays, due to their wide coupling bandwidth (>250 nm), compact size, and cost effectiveness, are an important building block for a number of crucial applications. These include clock signal distribution, multiwafer scale integration for ultrafast 3-D optical computers, optical backplanes, optical sensor probes, phased array antennae and surface plasmon resonant devices. In this section, we will described applicable scenarios.

5.1 Clock Signal Distribution

There are two types of signals that need to be routed in a large-scale optoelectronic system. They are data signals and clock signals. For a data signal, a high fan-out number is not a necessity in most cases. However, clock signal distribution does require a large number of fan-outs with minimum clock skew. In this case the multiplexed HOE is the device of choice. The combination of a microprism coupler and a multiplexed HOE, shown in

Figure 18 (holographic optical element), provides a massive fan-out clock signal. Note that the grating spacing Λ can be much smaller than that of direct fan-out using the waveguide/hologram combination directly. Smaller spacing of Λ drastically eases the fabrication process, and thus, the cost of the multiplexed hologram.

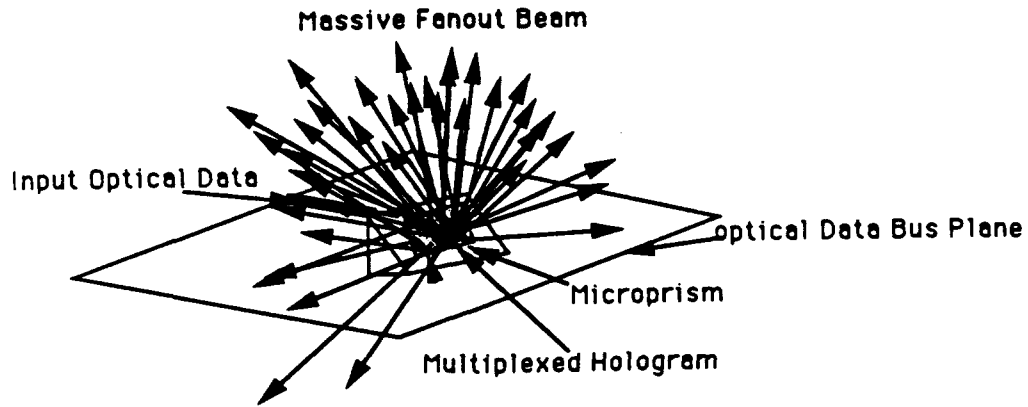


Figure 18
Clock Signal Distribution Using the Combination of MPC and Multiplexed HOE.

5.2 Multiwafer Scale Integration for Ultrafast 3-D Optical Computers

The success of this project will solve numerous interface problems associated with large-scale optoelectronic systems. Intra-chip, chip-to-chip, board-to-board, and system-to-system interconnects are some of the most important applications. Most importantly, the combination of an optical data bus and microprism arrays will efficiently solve the interface problem of coupling optical waves from single-mode waveguides to multi-mode fibers. A multi-wafer integrated package involving proposed MPCs is shown in Figure 19. An ultrafast speed 3-D optical computer can be realized based on this idea [23].

Note that the direction of the optical beams coming out of and thus into the microprisms can be precisely determined by designing the prism angles. The prism on board #1 is detailed in Figure 20 for vertical coupling.

The requirement of vertical coupling implies that

$$\theta_6 + \theta_8 = \pi/2 \quad (9)$$

It is easy to show, from waveguide theory, that

$$\theta_1 = \sin^{-1} (N_{\text{eff}}/N_p) \quad (10)$$

where N_{eff} and N_p are the effective index and prism index, respectively.

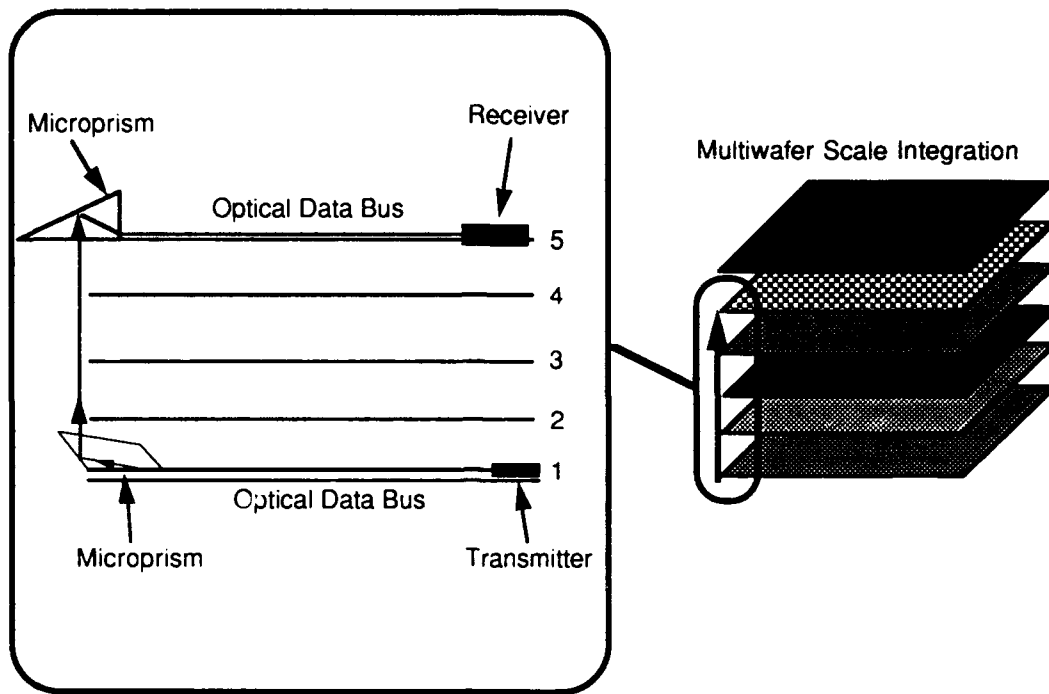


Figure 19
Multiwafer Scale Integration for Ultra-Fast 3-D Optical Computer Using MPC as the Interconnection Tool

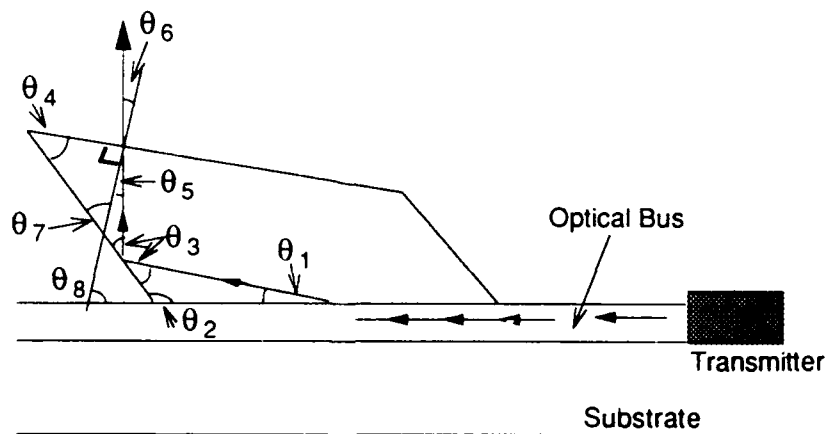


Figure 20
Vertical Coupling Using Microprism in Conjunction with Optical Bus

θ_2 and θ_4 are predetermined through prism design, i.e., preform fabrication. $\theta_3 = \pi - (\theta_1 + \theta_2)$, $\theta_7 = \pi/2 - \theta_4$, $\theta_8 = (\pi - \theta_7 - \theta_1 - \theta_3)$ and $\theta_5 = (\theta_7 - \theta_3)$. From the Fresnel equation, we have

$$\theta_6 = \sin^{-1} (N_p \sin(\theta_7 - \theta_3)) \quad (11)$$

We have thus determined all the numerical values of the angles needed to generate a vertical coupling. One crucial factor which needs to be taken care of in the prism design is that angle θ_3 has to be smaller than the total internal reflection angle, i.e., $\theta_3 < \cos^{-1} 1/N_p$.

The coupling prism for free space to optical bus coupling (board 5 of Figure 19) is further illustrated in Figure 21. The angle $\delta/2$ is the determining factor for successful coupling. From Figure 21, it is obvious that

$$\frac{\delta}{2} = \frac{1}{2}(\pi - \phi)$$

where

$$\phi = \sin^{-1} \left(\frac{N_{\text{eff}}}{N_p} \right) \quad (12)$$

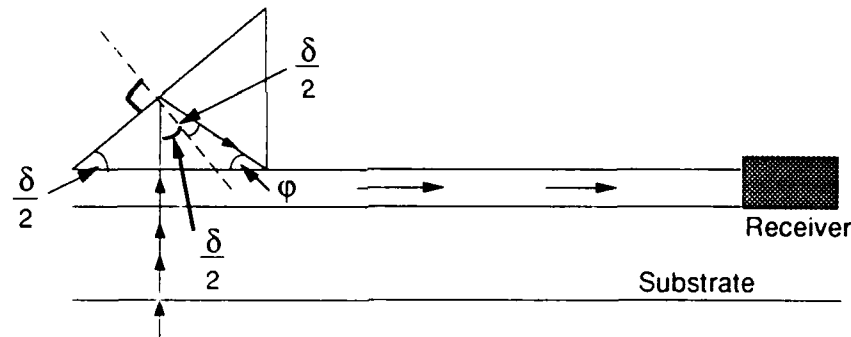


Figure 21
Microprism for Free Space-to-Optical Bus Coupling (Board 5 of Figure 19)

One precaution is that a high index prism N_p shall be chosen such that $\delta/2$ is larger than the critical angle. The substrate material for board 5 (Figure 19) shall also be transparent to the optical wavelength.

5.3 Miniaturized Sensor Probe

Another feasible application of the microprism is the miniaturized sensor probe. Advancements in optical sensors have greatly changed the system designer's concepts of ground-based and space-borne vehicles. The technology that is currently available for optical sensing probes is summarized in Figure 22 [24]. Lightweight and immunity to electromagnetic interference (EMI) and pulsing (EMP) effects make both intrinsic and extrinsic fiber optical sensors more attractive than any existing technology.

The microprism-based sensor probe is coated with "analytes" which are sensitive to parameters such as pressure and temperatures. A schematic drawing of the probe is illustrated in Figure 23 where 2 quarter pitch GRIN lenses are employed to collimate the optical wave coming out of and then into fibers. The spectrum of the optical source is dependent on the bandwidth and the sensitivity of the analyte. For instance, a YIG (Yttrium Iron Garnet) film can be used as an analyte for the electromagnetic sensor (based on the Faraday effect) using a laser diode (narrow band) working in the near infrared as long as an appropriate analyte is properly located.

<div>Parameter</div> <div>Technology</div>	Rotary Position	Linear Position	Angular Velocity	tachometer/ Shaft Speed	Linear Acceleration	Temperature	Pressure	Flow (Mass)	Voltage	Current	Flow (Volume)	Liquid Level	Pyrometer	Flame Sensor	Clearance	Proximity Switch	Vibration
TDM Digital Optical Code Plate	●	●					●										
WDM Digital Optical Code Plate	●	●															
Analog Gradient Filter Plate	●	●															
Beam Interrupt/Pulse Count	●	●		●													●
Microbend Modulated					●		●										●
Absorption Edge Shift						●											
Reflective Diaphragm						●	●	●			●				●	●	●
Near Total Internal Reflection												●					
Farady Effect						●				●							
Raman/Raleigh Backscatter						●											
Blackbody Radiation						●											
Passive IR Analysis						●							●	●			
Fabry-Perot Interferometer						●	●		●	●							
Phosphorescent						●											
Fluorescent						●											
E-O Diffraction Grating							●		●					●			●
Michelson Interferometer							●		●								
Mach-Zehnder Interferometer					●				●								●
Sagnac Interferometer			●			●											
Photo-Elastic							●										
Power-By-Light (PBL)	●	●				●										●	

Figure 22
Fiber Optic Sensor Technology Availability

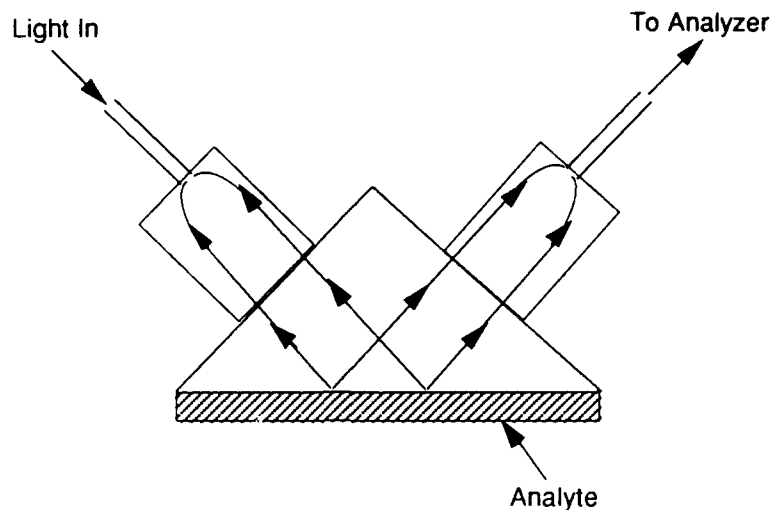


Figure 23
Microprism-Based Miniaturized Sensor Probe

5.4 Optically-Controlled Phased Array Antennas

A phased-array radar antenna to be implemented in the next generation Patriot missiles consists of anywhere from 1000 to 10000 [25] regularly spaced individual elements. Such a high degree of fan-out is beyond the limitations of current integrated optical interconnection networks.

To solve the problem described above, POC has demonstrated discrete integrated optical components. These components include a wide-band microprism coupler, polymer waveguides, highly multiplexed waveguide holograms, heterodyning of two optical signals, polymer waveguide lenses on Si and GaAs. To demonstrate an integrated optical system useful for both optical control of microwave and signal processing, the on-chip optical interconnection and processing network shown in Figure 24 can be used. The phase and intensity modulator arrays are based on POC's experience gleaned from a number of previous SBIR programs. Integrated optical circuits (IOC) of this type will be useful not only for the optical control of microwaves but also for optical signal processing. For example, we can also demonstrate an EO modulator array (Figure 24) and a vector-to-matrix multiplication module using a similar structure. By implementing the microprism array which is $\sim 100 \mu\text{m}$ or larger on the polymer waveguide surface, we are capable of efficiently interconnecting discrete electrooptic devices in different interconnection schemes.

5.5 Surface Plasmon Resonant Device Using a Microprism

Figure 25 shows the configuration that produces surface plasmon resonant absorption using the evanescent waves generated by a TIR prism.

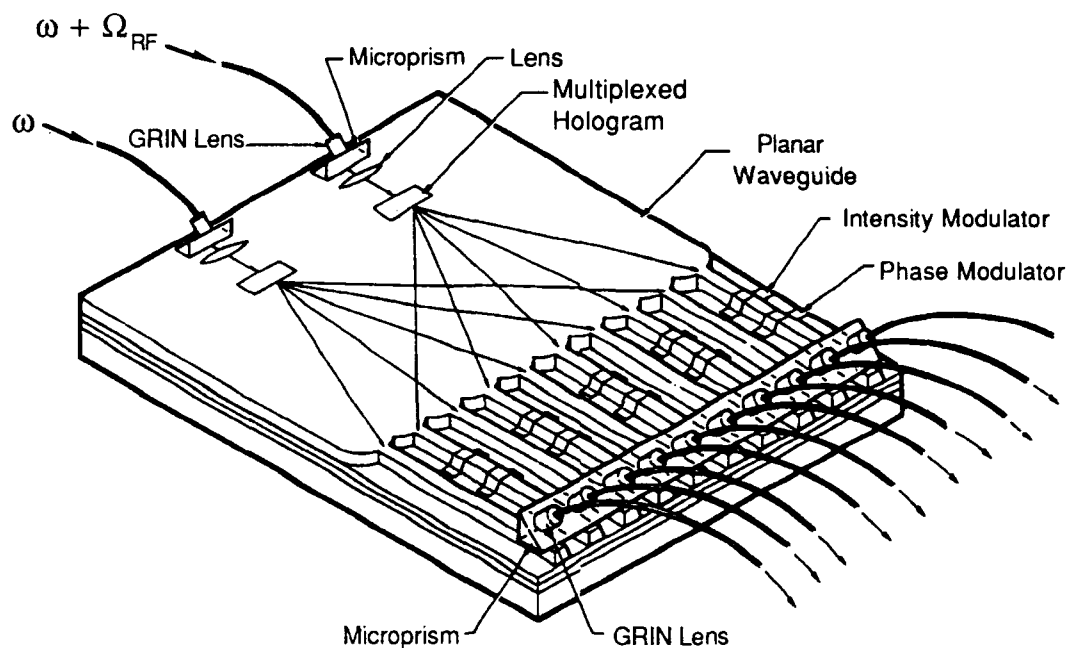


Figure 24
High Density Phase-Delay Lines Using Microprism Arrays in Conjunction with Integrated Optical Circuits

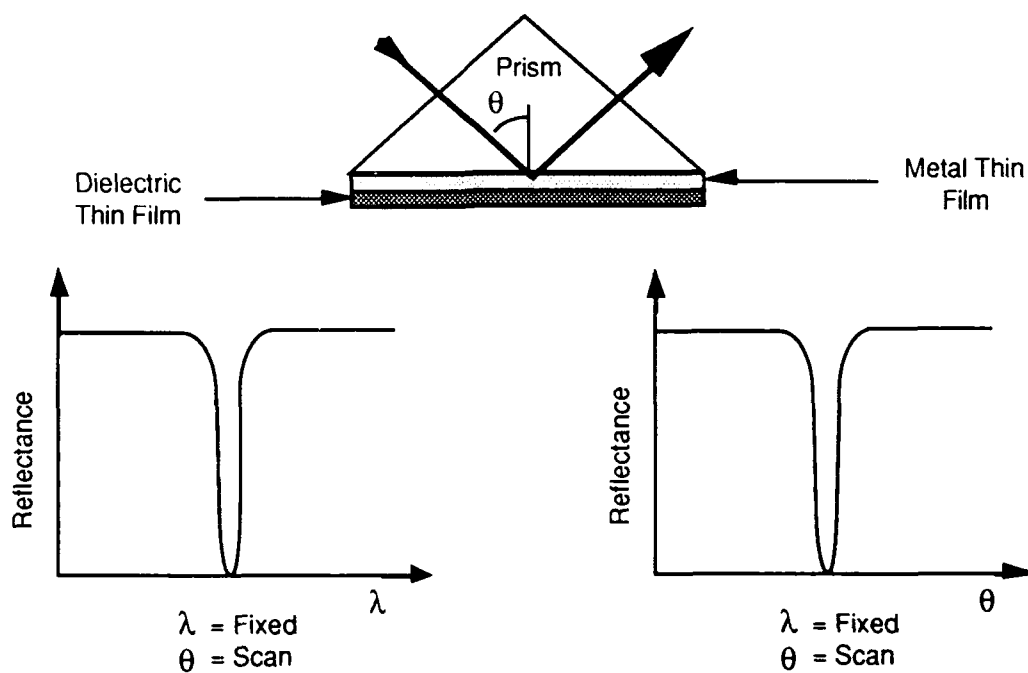


Figure 25
Surface Plasmon Resonant Device Based on Microprism

The temporal frequency ω of a surface plasmon polariton (SPP) in a metal-dielectric interface is related to its spatial frequency K by the dispersion relation

$$\omega_{SPP} = cK \left(\frac{1}{\epsilon_M} + \frac{1}{\epsilon_D} \right) \quad (13)$$

where c is the speed of light, ϵ_D the dielectric constant of the dielectric material, and ϵ_M is the dielectric constant of the metal given by the function

$$\epsilon_M(\omega) = 1 - \frac{\omega_p^2}{\omega^2} \quad (14)$$

where ω_p is the plasma frequency of the metal, typically corresponding to the ultraviolet wavelength of light. The dielectric constant ϵ_D of a dielectric material is the square of its refractive index. Figure 26 is a graph of Eq. 14, showing the line for ω_D , the free-space dispersion relation given by

$$\omega_D = \frac{cK}{\sqrt{\epsilon_D}} \quad (15)$$

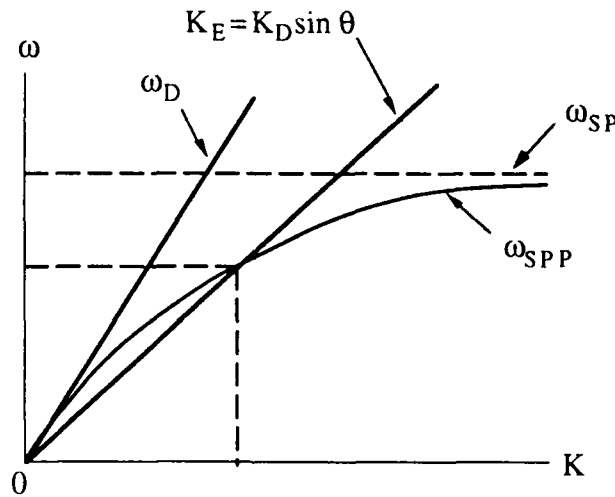


Figure 26
SPP Coupling to Evanescent Waves, with Free-Space Dispersion ω_D , Surface Plasmon Cutoff ω_{SP} and SPP Dispersion Curve ω_{SPP} . Dotted lines show the coupling condition.

At low spatial frequencies, the SPP frequency is just to the right of the ω_D line, then it turns through a knee to the asymptotic surface plasmon cutoff frequency

$$\omega_{SP} = \frac{\omega_p}{\sqrt{1 + \epsilon_D}} \quad (16)$$

The condition for energy transfer from light to an SPP is that both spatial frequency K and temporal frequency ω match. Because the SPP dispersion curve is to the right of that of

light freely propagating in the medium, direct excitation by that light is not possible. However, evanescent waves differ from freely propagating light because they propagate parallel to the dielectric interface and have a dispersion relation dependent upon the angle of incidence, θ , of light at the interface

$$K_E = K_D \sin \theta \quad (17)$$

When the line represented by this relation crosses the SPP dispersion curve, the evanescent waves will excite an SPP.

Because there is no discontinuity in the electric-field component parallel to the metal-dielectric interface, it cannot excite surface charges. Thus the SPP electric field is always normal to the surface and the magnetic field must always be parallel to it, so that surface plasmon polaritons propagate with the magnetic field in the plane of confinement (transverse magnetic (TM) polarization only). Thus, only the TM component of evanescent waves will excite SPPs, and only the TM component in a waveguide can be modulated in this way.

Experimental results of the surface plasmon resonant device are shown in Figure 27. A HeNe laser was employed for this demonstration. The resonant angle was provided by changing the angle θ (Figure 25). A variety of devices based on this concept can be imagined. High speed modulators and EM wave sensors are some of the most attractive ones.

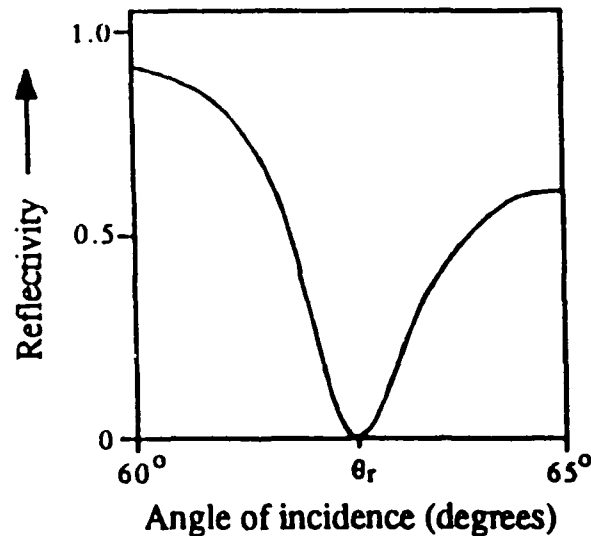


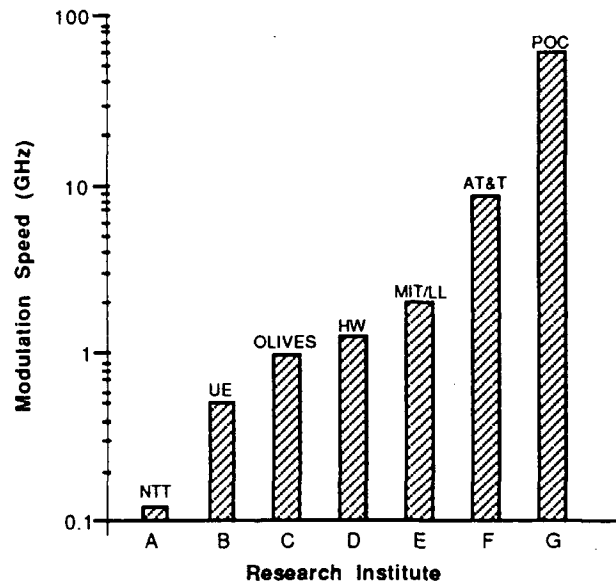
Figure 27
Measured Response of SPR as a Function of Incident Angle ($\lambda = 632.8 \text{ nm}$)

6.0 CONCLUSION

We have successfully demonstrated a microprism-based optical interconnection network for system wide communications. Microprisms with linear dimensions as small as $100 \mu\text{m}$ was successfully fabricated using both plate cutting and fiber drawing methods. Unlike conventional prisms, which need to be attached to the optical bus (waveguide) through

external elements such as clamps and optical adhesives, the microprisms reported herein were attached to the optical bus through van der Waals Force. No external instrument is needed to provide optimal coupling.

Two-dimensional interconnects using microprisms as the input and output couplers were demonstrated. Ten parallel channels were demonstrated simultaneously. The coupling efficiency variation for this 10-channel device is within $\pm 5\%$, which implies that a highly uniform gap between the microprism and optical bus was maintained. The coupling bandwidth from free space to the optical bus using a microprism coupler was further measured. A 3 dB bandwidth of >250 nm was experimentally confirmed. This is around two orders of magnitude larger than for holographic optical elements (HOEs). The most advanced demonstration for the Phase I program was the three dimensional board to board optical interconnect. A signal carrier bandwidth (baseboard) of 60 GHz with 22 dB signal to noise ratio, equivalent to 10^{-10} bit error rate (BER), was shown. This result makes POC the leading company for 3-D optical interconnects. (See Figure 28 for details.)



- NTT: Nippon Telegraph and Telephone Corporation
- UE: University of Erlangen (Germany)
- OLIVES: European Joint Program of Optical Interconnections for VLSI and Electronic Systems
- HW: Honeywell
- MIT/LL: MIT Lincoln Lab
- AT&T: American Telegraph and Telephone Corporation
- POC: Physical Optics Corporation

Figure 28
Demonstrated Modulation Bandwidth of Board-to-Board 3-D Optical Interconnects

Finally, the smallness and cost effectiveness of the proposed microprisms provide an array of highly feasible applications. These include clock signal distribution, multi-wafer scale integration for ultrafast 3-D optical computers, miniaturized sensor probes, optically controlled phased array antennas and surface plasmon devices.

The demonstrated features of microprisms were summarized in Table 1. The microprism features were compared to those of HOEs.

7.0 REFERENCES

1. Ray T. Chen, et al., "GaAs-GaAlAs Heterostructure Single-Mode Channel Waveguide Cut-off Modulator and Modulator Array", IEEE J. of Quantum Electron., QE-14, 539, 1987.
2. K. M. Johnson, et al., "Optical Computing and Image Processing with Ferroelectric Liquid Crystal", Opt. Eng., 26, 385, 1987.
3. F. Lin, "Integrated Optical Holographic Memory", Final Report to RADC, 1989.
4. Raymond K. Kostuk, et al., "Reducing Alignment and Chromatic Sensitivity of Holographic Optical Interconnects with Substrate-Mode Holograms", Applied Optics, 28, 4939, 1989.
5. J. W. Goodman, et al., "Optical Interconnects for VLSI Systems", Proc. IEEE, 72, 850, 1984.
6. Ray T. Chen, et al., "Integration of Holographic Optical Elements with Polymer Gelatin Waveguides on GaAs, LiNbO₃ Glass and Aluminum", Optics Lett., 14, 892, 1989.
7. F. Lin, et al., "Optical Multiplanar VLSI Interconnects Based on Multiplexed Waveguide Hologram", Appl. Opt., 29, 1126, 1990.
8. S. R. Forrest, Proc. IEEE, 75, 1488 (1987).
9. G. Kar, "Optical Waveguides: Fabrication and Drawing Standards," Photonic Spectra, December, 1985.
10. R. Ulrich, "Optimum Excitation of Optical Surface Waves," J. Opt. Soc. Am., 60, 1337 (1971).
11. R. T. Chen, Proc. SPIE, 1374 (1990).
12. R. T. Chen, M. R. Wang, G. J. Sonek, and T. Jansson, Optical Engr., 30(5), 622 (1991).
13. R. T. Chen, H. Lu, M. R. Wang, D. Robinson, and T. Jansson, accepted for publication in IEEE/OSA J. Lightwave Tech.
14. M. R. Feldman, S. C. Esener, C. C. Guest, and S. H. Lee, Appl. Opt., 27, 1742 (1988).

15. S. Kawanishi, A. Takada, and M. Saruwatari, IEEE/OSA J. Lightwave Technology, Vol. 7, No. 1, 92(1989).
16. K. L. Tan, R. M. Dia, D. C. Streit, L. K. Shaw, A. C. Han. M. D. Sholley, P. H. Liu, T. Q. Trinh, T. Lin, and H. C. Yen, IEEE Electron Device Let., 12, 23(1991).
17. L. K. Shaw, D. Brunone, T. Z. Best, B. Nelson, W. Jones, D. Streit, and P. Liu, in the Technical Digest of the 15th International Conference on Infrared and Millimeter Waves, 523 (1991).
19. S. Y. Wang IEEE D. M. Bloom, Electron. Lett., 19, 554 (1983).
20. R. T. Chen, Final Report to Army Harry Diamond Lab, Contract No. DAAL02-91-C-0034 (1991).
21. Andrew Yang, in Integrated Photonics Research, 1991, Technical Digest Series (OSA, Washington, DC, 1991), 590 and D. Z. Tsang, Proc. SPIE Vol. 1563-10 (1991).
22. J. W. Parker, in Topical Meeting on Optical Computing, 1990, Technical Digest Series (OSA, Washington, D. C.), 286.
23. M. J. Little and J. Grinberg, "The 3-D Computer: An Integrated Stack of WSI Wafers," Chapter 6 of Wafer Scale Integration, Klumer Academic Publisher, Boston, pp. 253-317 (1989).
24. Ray T. Chen, "Reconfigurable Switching Network for Multimode Fiber Arrays," Proc. SPIE Vol. 1338, 69 (1990)
25. N. Gupta, G. Simonis, and P. Ashley, "LiNbO₃ Integrated-Optics Demonstration of Optical Control of Microwave, " Proc. of SPIE, 1217 (1990).